AIAA JOURNAL
Vol. 40, No. 7, July 2002

Subcritical Flow Around Bluff Bodies

Mustafa Sarioglu* and Tahir Yavuz†
Karadeniz Technical University, 61080 Trabzon, Turkey

Results of experimental investigations of vortex-shedding frequencies and surface pressures of circular and square cylinders with the same hydraulic diameter are described. Pressure measurements on circular and square cylinders and hot-film measurements in the wakes were conducted. The range of Reynolds numbers was 1.3×10^4–2×10^5, which is characterized as subcritical flow regimes. Also, to reveal the combined influence of Reynolds number and angle of incidence on the pressure and spectral density distributions of velocities, experiments were carried out on square and rectangular cylinders for the angle of incidence in the range $0 \leq \alpha \leq 45$ deg. At zero incidence, pressure coefficients on the front and side faces of the square cylinder change considerably with Reynolds number, whereas as the angle of incidence increases to 30 deg, the effect of the Reynolds number seems to diminish. Spectral density distributions in the wake and surface pressures depend on Reynolds number and the angle of incidence. The variations of the strength of the spectral densities with Reynolds number in the wakes of circular and square cylinders show different characteristics. Variations of spectral density distributions and vortex shedding with Reynolds number, geometric dimensions of models, and angle of incidence are presented.

Nomenclature

C_p	=	pressure coefficient, $(P - P_{st})/\frac{1}{2}U^2$, dimensionless
C_{pc}	=	corrected pressure coefficient
D	=	cylinder diameter, m
E	=	anemometer output voltage, V
F	=	shedding frequency parameter (nondimensional frequency), $f_s h^2/\nu$ and $f_s D^2/\nu$
f_s	=	vortex-shedding frequency, Hz
H	=	height of the test section of the tunnel, m
h	=	height of the model, m
L	=	length of the model, m
P	=	surface pressure, N/m^2
P_{st}	=	static pressure in the test section, N/m^2
Re	=	Reynolds number based on h (or D), $\bar{U}h/\nu$ or $\bar{U}D/\nu$, dimensionless
Sr	=	Strouhal number, $f_s h/\bar{U}$ or $f_s D/\bar{U}$, dimensionless
t	=	time, s
U	=	freestream velocity, m/s
$\bar{U}$	=	mean velocity in x direction, m/s
$\overline{u^2}$	=	mean-square value of velocity fluctuations in x direction, m^2/s^2
W	=	width of the test section of the tunnel, m
w	=	width of the model, m
x, y, z	=	streamwise, lateral, and spanwise coordinates, m
α	=	angle of incidence, deg
ϵ	=	blockage ratio, D/H or h/H
θ	=	circumferential angle measured from the front stagnation point, deg
ν	=	kinematic viscosity, m^2/s
ρ	=	density of air, kg/m^3

I. Introduction

DETAILED information about flowfields around bluff bodies is of special interest for basic understanding of aerodynamics and aeroelastic instability and is of great importance in the study of aeroelastic instability. Circular and rectangular cylinders are frequently used as structures of members in numerous different areas in engineering. Circular and rectangular cylinders create different flowfields. The separation point on the circular cylinder varies with the Reynolds number, whereas it is generally fixed at the leading edges for rectangular cylinders. Despite the simplicity in geometries, the flows around these bluff bodies are actually very complicated. The flow characteristics are rather sensitive to factors such as freestream turbulence, model geometries, experimental environments, wind-tunnel blockage, model end conditions, alignment length-to-diameter ratio, surface irregularities, and incident angle for rectangular cylinders. The flow structure around a circular cylinder is a classical and important problem in fluid engineering. It is frequently associated with vortex shedding and flow instability, causing unsteady forces on the structures. Flow instabilities and periodic shedding of vortices from circular cylinders have been studied for over a century. Experimental and theoretical studies of circular cylinders have provided a large amount of data on pressure distribution, drag and lift coefficients, and vortex shedding. The lack of consistency in controlling second parameters, such as aspect ratio, freestream turbulence, surface irregularity, blockage ratio, etc., in different studies has made comparison difficult. These are the reasons why research in these areas started a few decades ago are still in progress today.

Wakes behind bluff bodies are so frequently encountered in engineering applications that research has been conducted in large numbers, and massive data have been accumulated. The subject of bluff-body flows has recently been receiving a great deal of attention (e.g., Refs. 1–19). This is largely because of its importance for energy conservation. For instance, large structures must be designed to avoid potentially disastrous wind-induced large-amplitude oscillations. There is a complex interaction between the turbulence and the flow past bluff structures, which leads to changes in the mean and unsteady wind loads. In addition, road vehicles must now meet stringent fuel-consumption requirements, which translate into a need for reduced aerodynamic drag. As first suggested by Roshko,[20] depending on the Reynolds numbers, at least three flow regimes around a nominally smooth cylinder can be identified: subcritical (purely laminar boundary-layer separation), supercritical (laminar separation followed by turbulent reattachment and eventual turbulent separation), and transcritical (transition to turbulence in the boundary layer occurring ahead of separation).

The characteristics of the flow around a smooth circular cylinder in the critical Reynolds number range were experimentally investigated by Farell and Blessmann[21] based on instantaneous mean pressure distribution measurements on the cylinder and hot-wire velocity fluctuation measurements in the cylinder wake. Two subregions were identified in the critical or lower transition: The first subregion ($1.5 \times 10^5 < Re < 3 \times 10^5$) is characterized by symmetric

Received 24 September 1999; accepted for publication 16 August 2001.

*Research Assistant, Department of Mechanical Engineering; sarioglu@ktu.edu.tr.
†Professor, Department of Mechanical Engineering.

pressure distributions, intense vortex shedding, and gradual and significant variations in characteristic parameters as Reynolds number increases. The second subregion (ending at $Re = 3.8 \times 10^5$) is characterized by intense flow oscillations associated with formation and bursting of laminar separation bubbles on one or both sides of the cylinder. The spectra of the velocity fluctuations in the second subregion show unsteady subranges, in general, with broadband peaks. Hence, different flow regimes around circular cylinder show different behaviors.

The effects of tunnel blockage and aspect ratio on the mean flow past a circular cylinder in the Reynolds number range $10^4 < Re < 10^5$ were investigated by West and Apelt.[22] They concluded that for the blockage ratios less than 6% the effects of the blockage on the pressure distribution and drag coefficient are small and that the Strouhal number is unaffected by blockage.

Blackburn and Melbourne[23] investigated the effects of the freestream turbulence and surface roughness on the sectional lift forces of a circular cylinder in the Reynolds number range 1×10^5–5×10^5. At higher turbulence intensities, effects consistent with a return to organized vortex shedding were observed at the upper end of the Reynolds number range. The flow past bluff structures is a classical and important problem in fluid engineering.

Mizota and Okajima,[24,25] using a tandem-type of hot-wire probe, measured the flow pattern around various rectangular cylinders, including a reversed flow region close to the cylinder, and confirmed that the changes of the patterns have close correlations with those of drag and lift forces and Strouhal numbers in the variation of the width-to-height ratio and the angle of incidence. As pointed out by Okajima,[26] for a sharp-edged body like a rectangular cylinder, where the separation points are fixed at the leading edges, the aerodynamic characteristics are said to be relatively insensitive to Reynolds number. At extremely low Reynolds numbers, flow around a rectangular cylinder is known to separate at the trailing edges rather than the leading edges. With an increase of Reynolds number, the flow separation at the leading edges will develop, and steady reattachments become impossible. Consequently, it is quite likely that there exists a certain range of the Reynolds number where the flow characteristics, Strouhal number in particular, of a rectangular cylinder alter remarkably.

Mukhopadhyay et al.[27] investigated the structure of confined wakes behind a square cylinder in a channel via the numerical solution of the unsteady Navier–Stokes equations. They simulated details of the flow phenomenon through numerical flow visualization.

It is common knowledge that flow around bluff bodies exhibits oscillatory behaviors, Kelkar and Patankar[18] computed the steady two-dimensional flow around a square cylinder at different Reynolds numbers and determined the onset of unsteadiness through a linear stability analysis of the steady flow.

Murakami et al.[8] analyzed velocity-pressure fields and wind-induced forces on and around a building model by means of numerical simulations. In their study, three types of well-known turbulence models, namely, k–ε eddy viscosity model, algebraic stress model, and large-eddy simulation have been used. They confirmed that results of the three-dimensional computation correspond very well to the experimental data, although the results of the two-dimensional computation include some significant discrepancies.

Calculations for the flow past a square cylinder at $Re = 2.2 \times 10^4$ placed at various distances from an adjacent wall, including the limiting case without wall influence, were conducted by Bosch and Rodi.[19] Two-dimensional unsteady equations were solved, which allows any periodic-shedding motion to be resolved. They concluded that the standard k–ε model was found to damp the shedding motion unrealistically so that shedding was suppressed at considerably larger gap widths than observed experimentally.

Calculations for the numerical simulation of the flow structure around a square cylinder in a uniform shear flow were conducted by solving the unsteady two-dimensional Navier–Stokes equations with a finite difference method by Hwang and Sue.[28] They investigated the effect of the shear parameter of the approaching flow on the vortex-shedding Strouhal number and the force coefficient acting on the square cylinder in the range of the shear parameter 0.0–0.25 at various Reynolds numbers ranging from 5×10^2 to 1.5×10^3. The effect of shear rate on the Strouhal number and the force acting on the cylinder has a tendency to reduce the oscillation. The Strouhal number tends to decrease as the shear rate increases, but shows no significant change at low shear rate.

The present study is an experimental investigation of the instabilities around circular and rectangular cylinders to assist in understanding the near-wake vortex dynamics. Pressures on circular and square cylinders with the same hydraulic diameters were measured, and hot-film measurements in the wakes were made. The range of Reynolds numbers was between 1.3×10^4 and 2.0×10^5, which is characterized as a subcritical flow regime. Measurements of spectral density distributions in the wakes and surface pressure coefficients were carried out to reveal the differences of the influence of Reynolds numbers on the patterns of separated shear layers and vortex formations about these two models. Also, the combined influences of Reynolds number and angle of incidence on pressure distributions and vortex formations around square and rectangular cylinders were determined. The variations of spectral density distributions in the wakes and vortex-shedding characteristics with Reynolds number, geometric dimensions of models, and angle of incidence are discussed in detail.

II. Instrumentation and Experimental Procedure

The experiments were conducted in the test section of a low-speed, open-return wind tunnel in the Department of Mechanical Engineering at the Karadeniz Technical University. The test section that measures 289 mm wide, 457 mm high, and 1830 mm long follows the contraction section. The two side Plexiglas® walls of the test section are tapered with a divergence angle of 0.3 deg on each side to give constant static pressure and to compensate for boundary-layer growth along the tunnel axis. A circular diffuser is connected to the test section through a transition section, where rectangular shape of the test section changes to the circular shape of the diffuser. At the maximum tunnel speed of about 36 m/s, the freestream turbulence intensity was about 0.15%; the turbulence intensity was higher at low tunnel speeds, about 0.4% at 5 m/s, which is the lowest speed used in the present study. The uniformity of the velocity in test section was about 0.2%. The wind tunnel and test section are shown in Fig. 1. The circular wooden cylinder model with a diameter of 50 mm and three rectangular wooden cylinder models with width-to-height ratios $w/h = 0.5$, 1.0, and 2 were used. The models were placed horizontally at midheight in the test section (Fig. 2), which is 400 mm downstream from the end of the contraction. With $w/h = 0.5$, 1.0, and 2.0, the blockage ratios of the rectangular cylinders were 17.51, 10.94, and 8.75%, respectively, at 0-deg incidence, and the blockage ratio of the circular cylinder was 10.94%. Each model was supported outside the test section to eliminate any transmission of tunnel vibrations. The rectangular cylinders used were tested at incidence angles of 0, 10, 20, and 30 deg. At these angles of incidence, the geometric blockage ratios varied from 10.94 to 14.95% for the square cylinder ($w/h = 1.0$).

Pressures were only measured on the square and the circular cylinders. The coordinate system, location of the models, and pressure taps on the models are shown in Fig. 2. Coordinates are defined with the z axis in the spanwise direction and the x axis in the streamwise direction. For the circular cylinder, 18 pressure taps were positioned circumferentially on the surface of the cylinder at the measuring station of $z/D = 0$, shown in Fig. 2b. In Fig. 2b, θ is circumferential angle measured from the forward stagnation point on the cylinder. For the square cylinder (Fig. 2c), there are four taps on the front surface, three taps on the back surface, and six taps on each of the side surfaces. Because the back surface is not important, only a few taps are located on this surface.

The tap opening diameter was 1 mm. The pressure taps were connected via 1-mm-internal-diameter plastic tubing to a pressure transmitter. Depending on the pressure levels, two capacitance-type pressure transmitters were used.

A TSI hot-film anemometer, Model IFA 100, was used for velocity measurements. A hot-film probe was placed at various locations in the wakes of the cylinders. Thermal-Pro Software for IFA 100, ADCWIN-4, was used to display the statistical results in the wakes of the models. The experimental uncertainty in the measurement

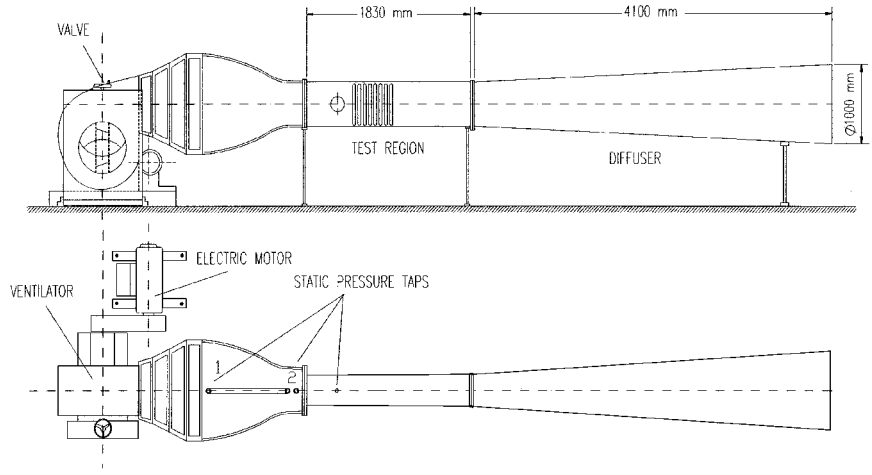

Fig. 1 Low-turbulence wind tunnel and test section.

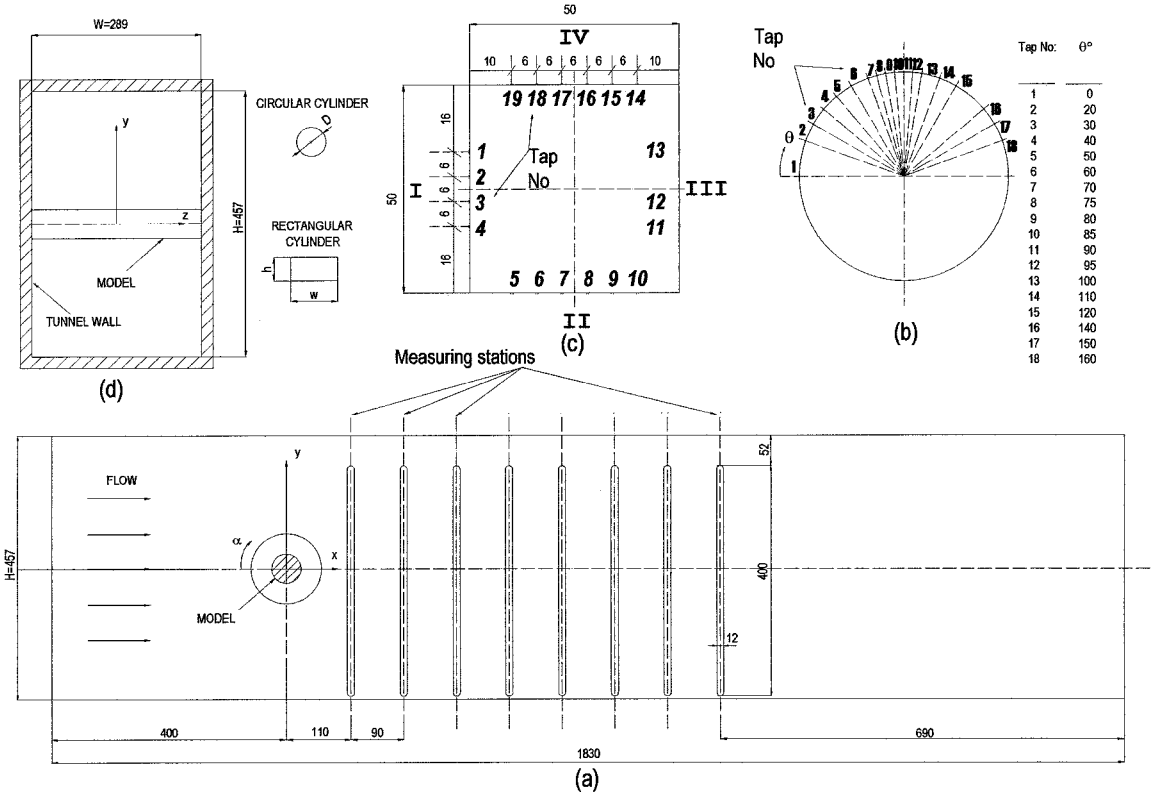

Fig. 2 Coordinate system; location of the models and pressure taps on the models; scale in millimeters.

of velocity was determined to be less than ±1%, whereas that of pressure was determined to be less than ±5%.

III. Experimental Results and Discussion

A. Velocity and Turbulence Intensity Measurements

Velocity and turbulence intensity profiles at various stations in the wakes of the circular and square cylinders having same hydraulic diameters of 50 mm were measured. Three Reynolds numbers, based on the hydraulic diameter, 1.467×10^4, 6.6539×10^4, and 1.30542×10^5, were considered.

Time histories of velocity fluctuations obtained for the circular cylinders at two downstream stations, $x/D = 2.2$ and 4.0, and at three locations, $y/D = 0.3$, 0.5, and 1.5, for each station are shown in Fig. 3. For the smallest Reynolds number, 1.467×10^4, the oscillations of the velocity fluctuation are not seen to appear. As the Reynolds number increases, oscillations frequency and amplitude of the velocity fluctuations increase, and the randomness characteristics of turbulence develop at a roughly equal rate throughout the transition region. Correspondingly, the timescale of fluctuations becomes continuously shorter. When the time histories of the velocity fluctuations obtained at the locations $x/D = 2.2$, $y/D = 1.5$ and $x/D = 4.0$, $y/D = 1.5$ are compared (Figs. 3a and 3b), the amplitudes of the velocity fluctuations are nearly disappearing at $x/D = 2.2$, $y/D = 1.5$, whereas farther downstream, $x/D = 4.0$, $y/D = 1.5$, there are noticeable oscillations and amplitude of the velocity fluctuation. This means that the width of the wake increases in the downstream direction.

Turbulence intensity profiles obtained at three different stations, $x/D = 2.2$, 5.8, and 14.8, in the wakes of the circular and square cylinders for the Reynolds numbers based on hydraulic diameter, 1.467×10^4, 3.6528×10^4, and 1.30542×10^5, are shown in Figs. 4 and 5, respectively. As shown in Fig. 4, for the circular cylinder, there are two peaks in the turbulent intensity profiles near the center of the wake at small x/D value ($x/D = 2.2$), whereas turbulent intensities have parabolic profiles at larger x/D values in the range of Reynolds number tested. At $x/D = 2.2$, turbulent intensity profiles

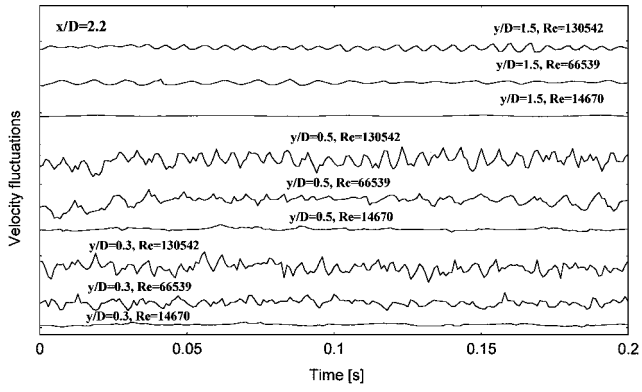

a)

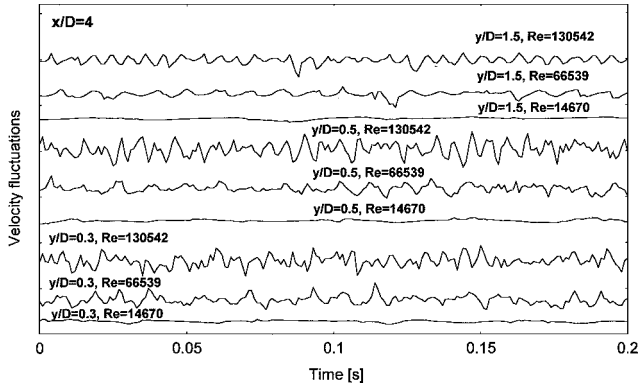

b)

Fig. 3 Time histories of velocity fluctuation at a) $x/D = 2.2$ and b) $x/D = 4.0$.

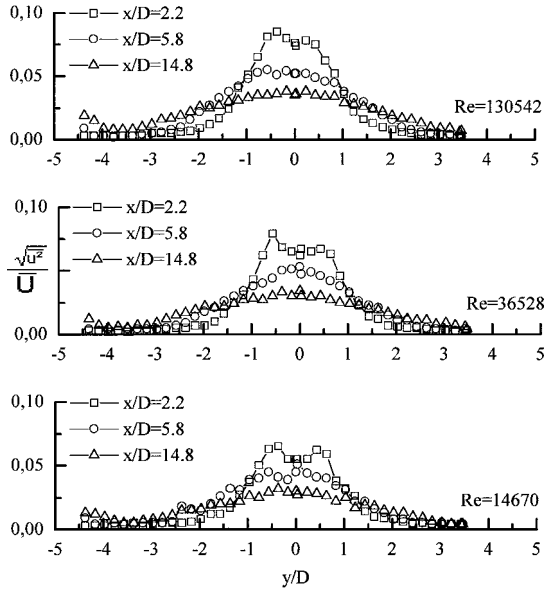

Fig. 4 Turbulence intensities at three different x stations behind circular cylinder for Reynolds numbers.

have maximum values approximately at $y/D = \pm 0.5$ due to a pair of standing eddies near the model in the wake. At $x/D = 5.8$ and 14.8, turbulent intensities have parabolic profiles and have maximum values at the center of the wake, $y/D = 0$. As expressed in the study of Ilday et al.,[29] it is seen that the peaks on the turbulence intensity profile correspond to the points on which the mean velocity gradient has the minimum values. This is due to the enhanced mixing at those points. It is also seen that the turbulence intensity profiles become asymmetric as the Reynolds number is increased

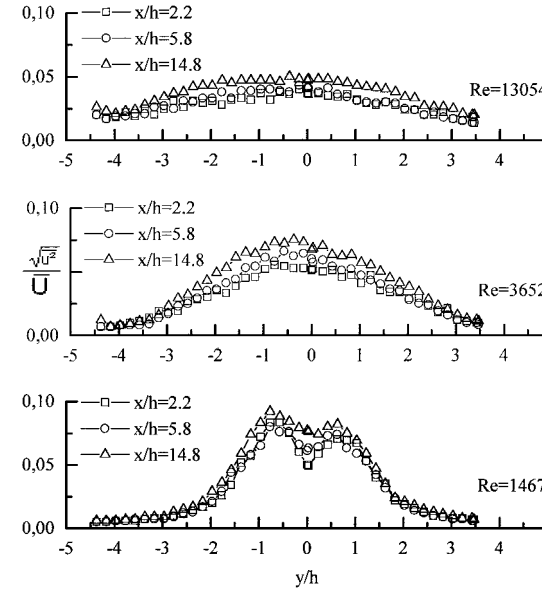

Fig. 5 Turbulence intensities at three different x stations behind square cylinder for Reynolds numbers.

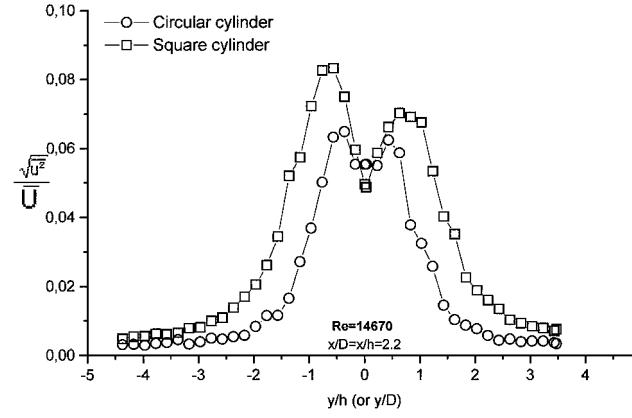

Fig. 6 Turbulent intensity profiles in the wakes of circular and square cylinders.

from 1.467×10^4 to 3.6528×10^4 and continues to be asymmetric after that. This might be due to the experimental error.

For the square cylinder (Fig. 5) at $Re = 1.467 \times 10^4$, as for circular cylinder, the turbulence intensity profiles determined at three stations, $x/h = 2.2$, 5.8, and 14.8, have two peaks. As the Reynolds number increases to 3.6528×10^4, these two peaks diminish, and turbulence intensities have maximum values on the centerline of the wake. Hence, when Figs. 4 and 5 are compared, as the Reynolds number increases, the flowfields about the circular and square cylinders show different characteristics. At the same Reynolds number, the width of the wake for the square cylinder is larger than that of the circular cylinder, as shown in Fig. 6.

The width of the wake for the square cylinder does not seem to vary with the Reynolds number. This is because the flow separates from the leading edges of the square cylinder and does not vary with the Reynolds number, whereas the width of the wake for the circular cylinder varies with the Reynolds number due to the separation points' dependence on the Reynolds number.

B. Mean Pressure Distributions

The pressure distributions on the surface of the cylinder were obtained in the Reynolds numbers range 1.6×10^4–1.34×10^5. The pressure coefficient C_p was defined as $C_p = (P - P_{st})/\frac{1}{2}\rho U^2$. Results are presented in Fig. 7. As seen, the pressure coefficient C_p varies with θ in the front of the cylinder and becomes considerably uniform on the rear side. The maximum negative pressure coefficient occurred before the apex of the cylinder at $\approx\theta = 70$ deg.

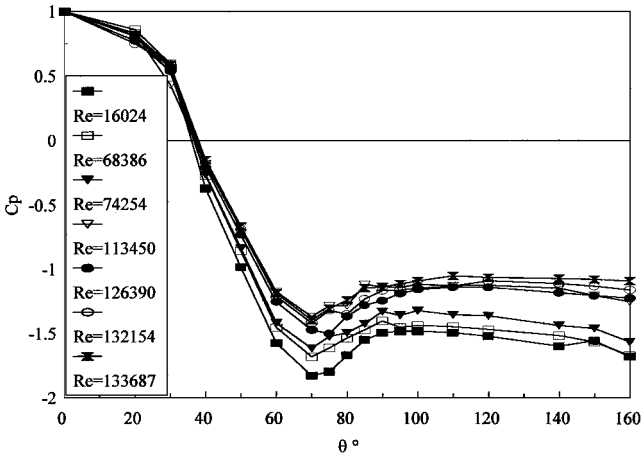

Fig. 7 Pressure coefficient C_p as a function of circumferential angle θ for various Reynolds numbers.

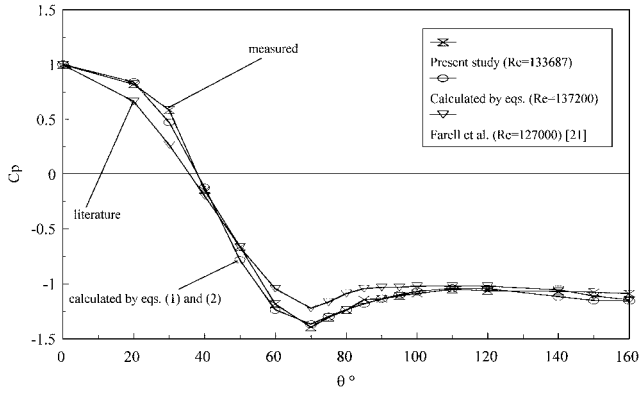

Fig. 8 Comparisons of pressure coefficient on the circular cylinder model.

Two empirical relations about pressure coefficient C_p depending on Reynolds number Re and circumferential angle θ, for $0 \le \theta \le 70$ deg were determined as

$$C_p = -6.1(\theta^{3.13}/Re^{0.026}) - 5.27\sin(1.55 + \theta^{2.724}) + 6.2745 \quad (1)$$

and for $70 < \theta \le 160$ deg as

$$C_p = -(0.06/\theta^{0.53})Re^{0.238} - 0.132\sin(2.059 + \theta^{1.65}) + 6.2 \times 10^{-6}Re - 0.01\ln\left(\sqrt{Re}\right) + 1.56\theta - 0.77\theta^2 + 0.1234\theta^3 - 2.28 \quad (2)$$

in which θ is in radians.

These formulas are valid in the range $1.6 \times 10^4 \le Re \le 1.34 \times 10^5$ and represent the experimental data with 99% accuracy. Comparisons are shown in Fig. 8 along with some data from the literature. Discrepancies among the data might be due to the different blockage ratios.

Because the tunnel blockage ratio is about 10.94%, correction for the blockage effect is necessary. In this study, $C_{pc} = 1 - (1 - C_p)/(1 + \epsilon)^2$, which is given by West and Apelt,[22] was adopted to account for the blockage effect. Figure 9 shows corrected and measured pressure coefficients for $Re = 1.6024 \times 10^4$. In Fig. 9, it is seen that blockage effect increases with increasing the circumferential angle and reaches almost the constant value of 29% after $\theta = 70$ rad.

Pressure distributions C_p on the square cylinder were obtained in Reynolds numbers, based on the model height, which is the hydraulic diameter, ranging from 1.4×10^4 to 1.3×10^5 with the incidence angles from 0 to 30 deg. Figure 10 shows pressure distributions on the cylinder surface for two incidence angles, 0 and 30 deg. In Fig. 10, areas I, II, III, and IV correspond to the front, bottom, back, and upper surfaces of the model, respectively. It can be seen that, at the incidence angle of 0 deg, the Reynolds number has no

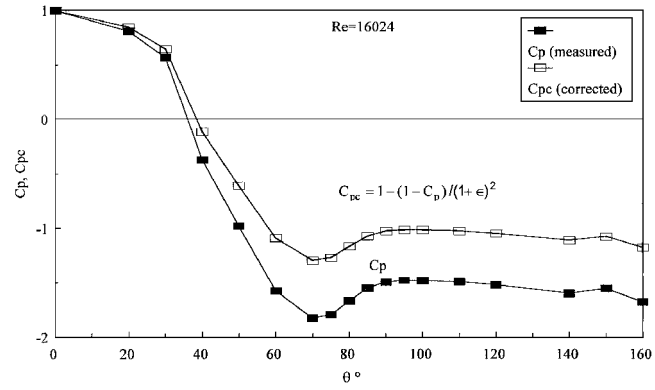

Fig. 9 Surface pressure coefficient on the circular cylinder model with and without blockage correction for $Re = 1.6024 \times 10^4$.

discernible effect on the pressure coefficient distributions on the front face (part I). However, the pressure distributions on the side and rear are affected by Reynolds number. As shown in Fig. 10, negative pressure coefficients were obtained, especially on the bottom and upper surfaces of the model. This may be caused by the accelerated two-dimensional high velocity producing flow separations at the side faces, as mentioned in the study of Murakami et al.[8] Increasing Reynolds number increases the pressure coefficients on these surfaces.

Large eddies form in the lee of the model and produce a large wake and low pressure on the leeward wall. When the angle of incidence was increased from 0 to 30 deg, the pressures on the bottom surface (part II) increased considerably, whereas pressure level on the front surface (part I) slightly increased due to the compression effects in these regions. The pressure levels on the other surfaces remained almost constant. Increase in Reynolds number does not cause considerable increase in pressure coefficient distributions on the surfaces of the model at the incidence angle of 30 deg.

C. Spectral Measurements

Spectral density distributions of velocities in the wake of the circular and square cylinders are calculated from the hot-film signals. As is known, in the spectra, spectral peaks reflect vortex shedding. Spectral density distributions of velocities have been determined at various locations in the wakes of the models.

As seen in Fig. 11, which shows results at $x/D = 2.2$, for the circular cylinder, for smallest Reynolds number, 1.6279×10^4, two dominant peaks in the spectra occur at $y/D = 0.3$ and 1.0 (Fig. 11a), whereas for higher Reynolds numbers, 6.6539×10^4 and 1.23355×10^5, only one dominant spectral peak occurs at $y/D = 0.5$ (Figs. 11b and 11c). Spectral peaks diminish in the spectra in the region $y/D \ge 1.5$.

At $x/D = 2.2$, the magnitudes of the peaks obtained at $y/D = 0.5$ increase with increasing Reynolds number, but they decrease with increasing Reynolds number at $y/D = 1.5$. However, farther downstream at $x/D = 4.0$, the magnitude of the spectral peaks detected at two locations $y/D = 0.5$ and 1.5 decrease with increasing Reynolds number. These points are shown in Fig. 12. Hence, depending on the locations at which the spectral measurements take place, the magnitudes of the spectral peaks vary with the Reynolds number. Notice from Figs. 12 that the vortex-shedding frequency increases with increasing Reynolds number.

Spectral density distributions obtained in the wake of the square cylinder with zero angle of attack are shown in Fig. 13. Variations of the spectral peaks with Reynolds number obtained at various locations in the wake show different characters. At $x/h = 2.2$, spectral peaks decrease with increasing Reynolds number at $y/h = 0.5$ and 1.5 (Figs. 13a and 13b). However, at $x/h = 4.0$, which is farther downstream in the wake, the spectral peaks increase with increasing Reynolds number at the same locations considered earlier (Figs. 13c and 13d). The same character of the spectral peaks was determined for the circular cylinder at $x/D = 2.2$, $y/d = 0.5$ (Fig. 12a).

Spectral density distributions of velocities obtained in the wake of the square cylinder were determined with incidence angles of

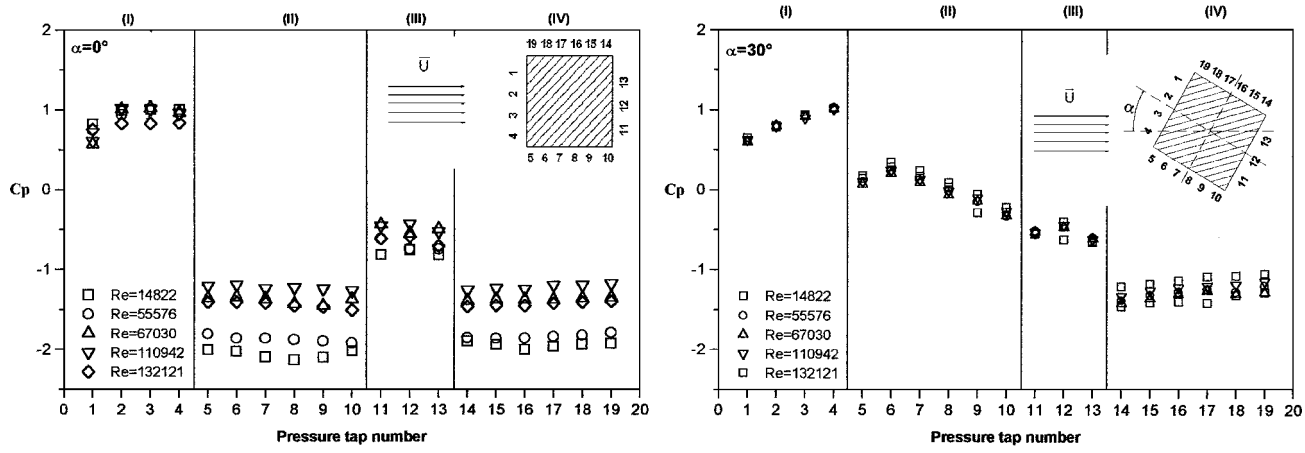

Fig. 10 Surface pressure distributions on square cylinder model for five different Reynolds numbers in the incidences $\alpha = 0$ and 30 deg.

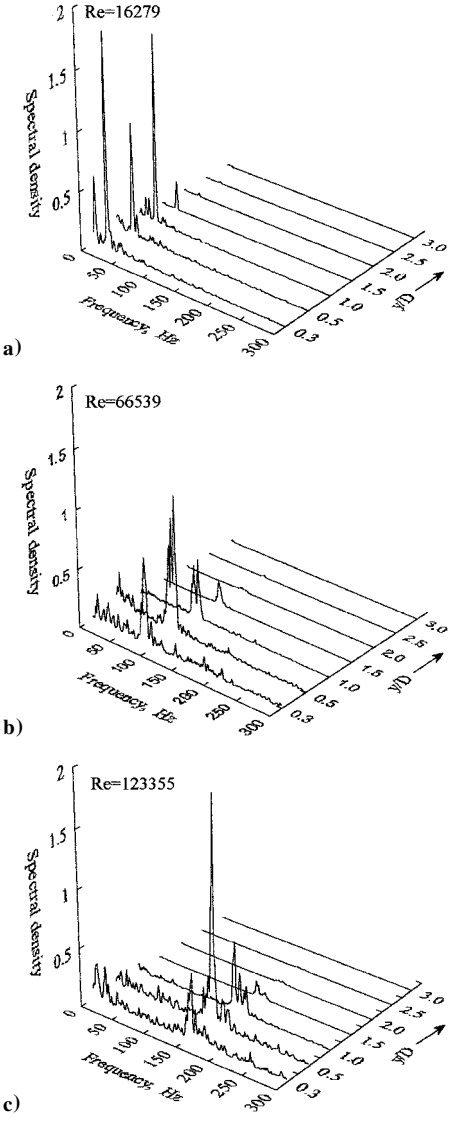

Fig. 11 Spectral densities of velocities vs *y/D* at *x/D* = 2.2 in the wake of the circular cylinder.

0, 10, and 30 deg. The definition of the angle of incidence is also shown in Fig. 2. As indicated before, the dominant peak in the spectra is the one associated with the vortex-shedding frequency. Results are presented in Figs. 14–16. As shown in Figs. 14–16, the intensities of the spectral peaks that represent the vortex shedding first increase with increasing y/h, reach the maximum values at some value of y/h, and then decrease with increasing y/h. Spectral peaks diminish considerably after $|y/h| \geq 2.5$.

At 0-deg incidence, the intensity of the spectral peaks has its maximum value at $y/h = 1.0$ and then decreases with increasing y/h. Spectral peaks did not appear after approximately $y/h \geq 2.5$ (Fig. 14), whereas in the wake of the circular cylinder with the same hydraulic diameter, the spectral peaks did not appear after approximately $y/D \geq 1.5$. This is because the wake of the circular cylinder is narrower than that of the square cylinder due to the different shape and locations of the separation points.

At 10-deg incidence, maximum spectral peaks were detected at $y/h = 1.0$ (Fig. 15). As Reynolds number increases, some subharmonic peaks appear in the spectra.

At 30-deg incidence, at the smallest Reynolds number, the maximum spectral peak was detected at $y/h = 0.5$ (Fig. 16). As the Reynolds number increases to 6.6539×10^4, two maximum spectral peaks were detected at $y/h = 0.5$ and 1.5, and as Reynolds number increases to 1.23355×10^5, only one maximum spectral peak was detected at $y/h = 1.0$.

The effect of the angle of incidence on the spectral density distributions are shown in Figs. 17 and 18 for three Reynolds numbers determined at the positive and negative sides in the wake of the square cylinder. In Fig. 17, which shows the spectral density distribution in the positive side of the wake, for $Re = 1.6 \times 10^4$ at $\alpha = 5$ deg, no spectral peaks appeared. The spectral peak increases with increasing the angle of incidence and reaches to its maximum at $\alpha = 30$ deg. For Reynolds numbers 6.65×10^4 and 1.23×10^5, the smallest spectral peaks were detected at $\alpha = 10$ deg and reached a maximum at $\alpha = 30$ deg. In Fig. 18, which shows the spectral density distribution in the negative side of the wake, the spectral peak increases with the angle of incidence. Spectral peaks were detected at all angles of incidence considered. Also, there are some subharmonic peaks in the spectra at $\alpha = 10$ and 20 deg. As noted by Obasaju,[12] they may have been caused by an interaction between a vortex and a trailing-edge corner.

Vortex-shedding frequency is commonly normalized by using the cylinder diameter and the approaching velocity, thus forming the Strouhal number $Sr = f_s D/\bar{U}$. Sometimes in the literature, vortex shedding is represented by the nondimensional frequency (the shedding-frequency parameter) $F = f_s D^2/\nu$, which represents the product of Reynolds and Strouhal numbers.

The Strouhal numbers vs Reynolds number obtained for the circular cylinder and some results determined by other investigators are compared in Fig. 19. As shown, the Strouhal number decreases slightly with increasing Reynolds number. Among the data shown, there are some discrepancies. These discrepancies might be due to the different blockage ratios in various works. The blockage ratios were 16.67, 11.9, 9, and 6.5% in the experiments of Achenbach and Heinecke,[30] Farell and Blessmann,[21] West and Apelt,[22] and Bearman,[31] respectively, whereas it was 10.94% in the present study.

Apart from the square cylinder, several experiments have been conducted on a rectangular cylinder with aspect ratios of $w/h = 0.5$ and 2.0. Results obtained along with some data from the literature are presented in Fig. 20. Among the data shown, there are some

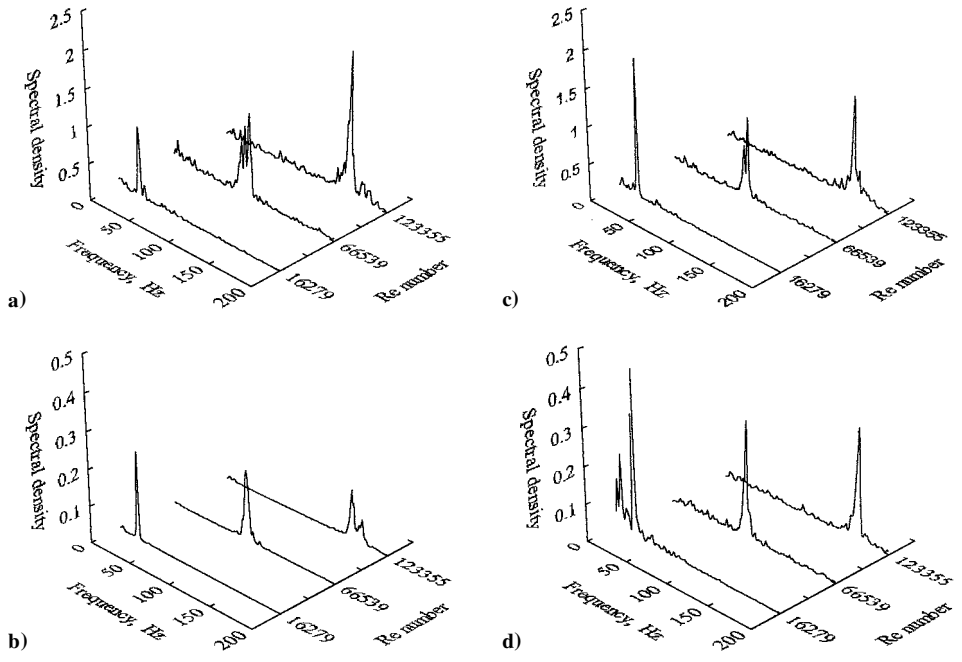

Fig. 12 Spectral densities of velocities vs Reynolds number in the wake of circular cylinder at positions a) $x/D = 2.2$, $y/D = 0.5$, b) $x/D = 2.2$, $y/D = 1.5$, c) $x/D = 4.0$, $y/D = 0.5$, and d) $x/D = 4.0$, $y/D = 1.5$.

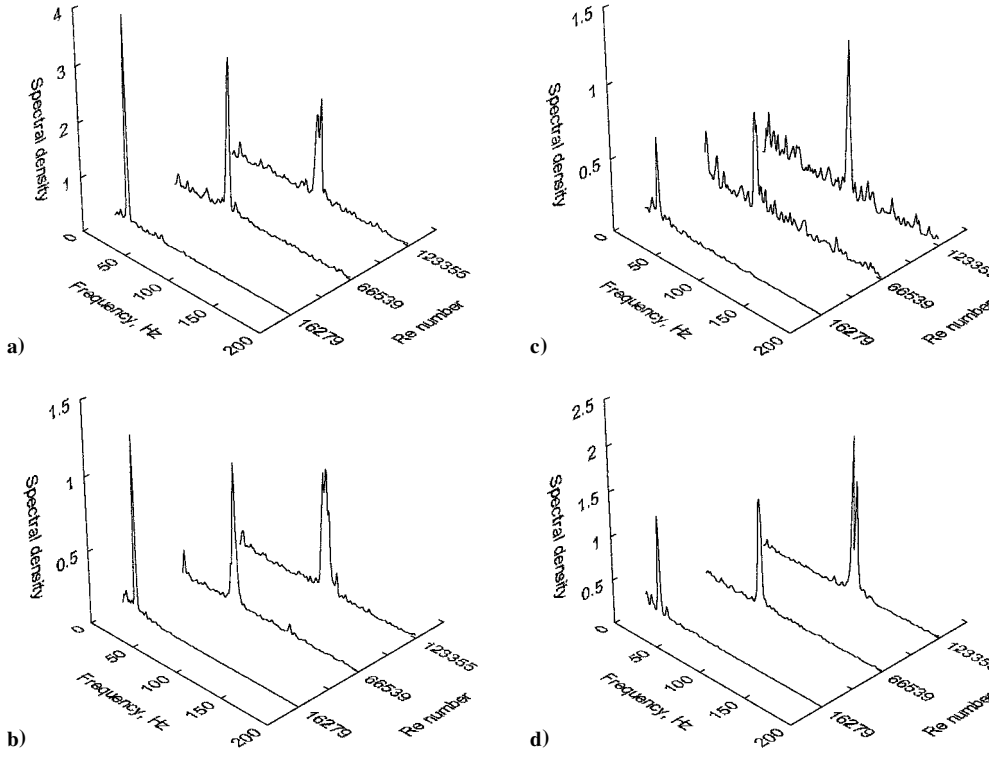

Fig. 13 Spectral densities of velocities vs Reynolds number in the wake of the square cylinder at positions a) $x/h = 2.2$, $y/h = 0.5$, b) $x/h = 2.2$, $y/h = 1.5$, c) $x/h = 4.0$, $y/h = 0.5$, and d) $x/h = 4.0$, $y/h = 1.5$.

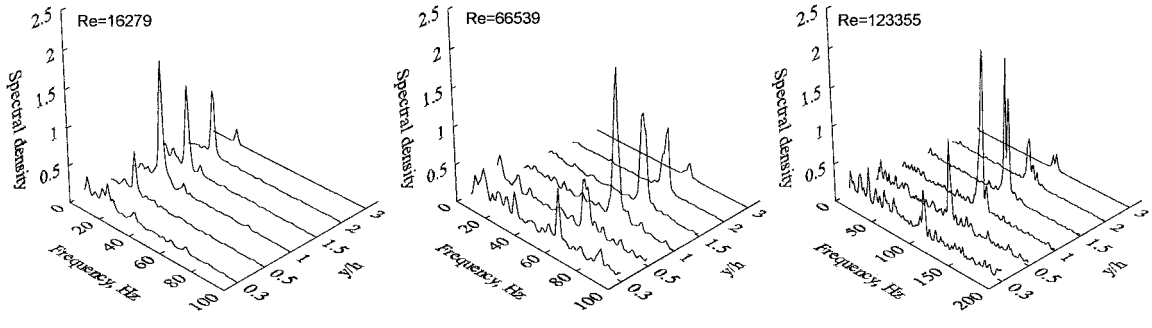

Fig. 14 Spectral densities of velocities vs y/h at $x/h = 4$ in the wake of the square cylinder at 0-deg incidence.

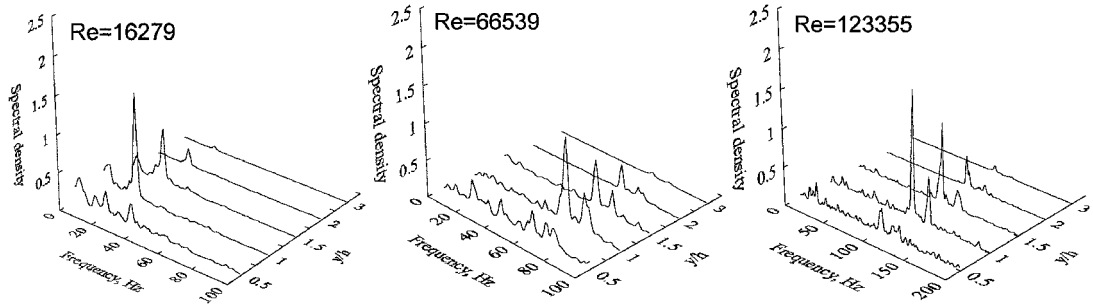

Fig. 15 Spectral densities of velocities vs y/h at $x/h = 4$ in the wake of the square cylinder at 10-deg incidence.

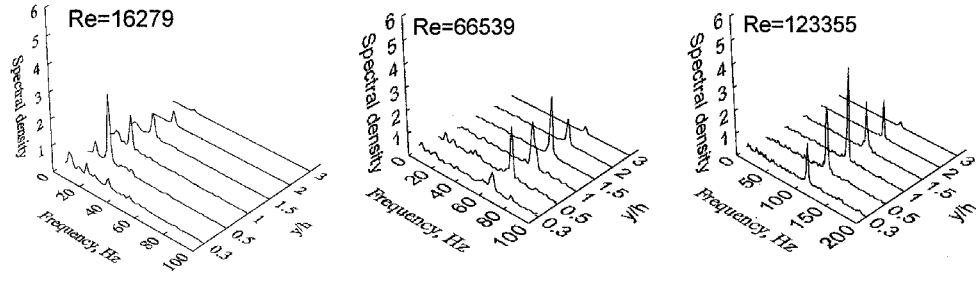

Fig. 16 Spectral densities of velocities vs y/h at $x/h = 4$ in the wake of the square cylinder at 30-deg incidence.

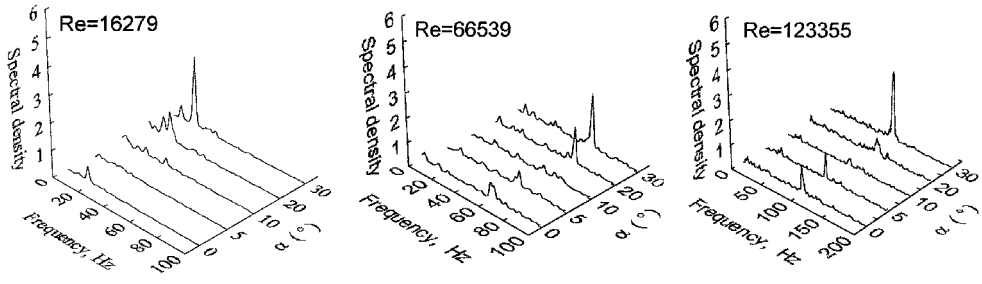

Fig. 17 Spectral densities of velocities vs angle of incidence α for three Reynolds numbers at $x/h = 4$, $y/h = 0.5$ in the wake of the square cylinder.

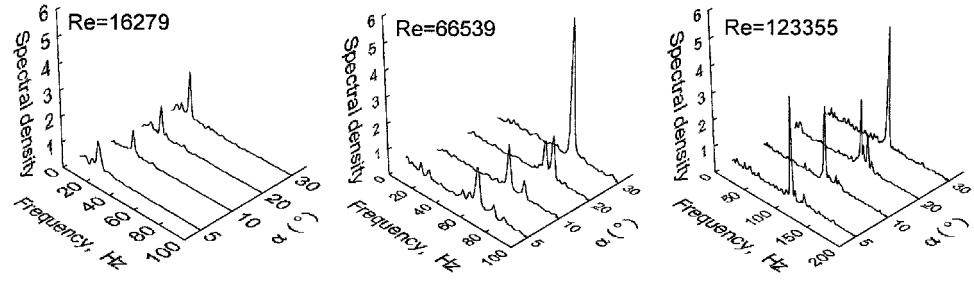

Fig. 18 Spectral densities of velocities vs the angle of incidence α for three Reynolds numbers at $x/h = 4$, $y/h = -0.5$ in the wake of the square cylinder.

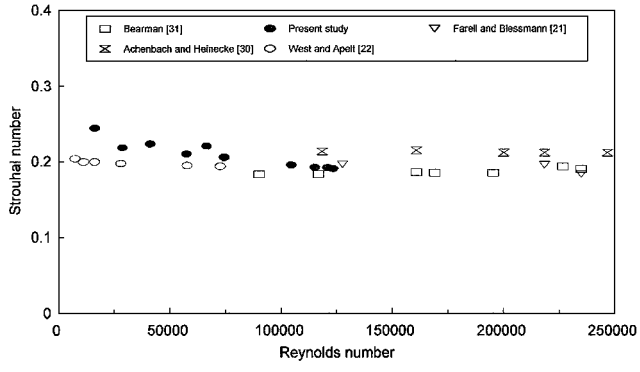

Fig. 19 Strouhal numbers vs Reynolds numbers for the circular cylinder.

discrepancies. It might be due to the different blockage ratios in various studies.

The effects of aspect ratios w/h on Strouhal number for rectangular cylinders are determined and shown in Fig. 21. As shown in Fig. 21, Strouhal number slightly decreases with increasing w/h ratios, and results are in good agreement with those of Nakaguchi et al.[32] and Nagano et al.[33] Work conducted by Nakaguchi et al.[32] and Bearman and Trueman[10] on rectangular cylinders showed that there exists a critical ratio of body dimensions $(w/h)_{cr}$, where drag coefficient reaches a maximum value. Nakaguchi et al.[32] and Bearman and Trueman[10] explain that two opposite effects occur for $w/h < (w/h)_{cr}$ and $w/h > (w/h)_{cr}$. Calculations by Park[16] for rectangular cylinders show that the Strouhal number increases with w/h for $w/h < 0.6$ and decreases for $w/h > 0.6$. This means that $(w/h)_{cr}$ can be considered to be about 0.6. In the present experiments, w/h ratios varied from 0.5 to 2.0, which are considered

to be $w/h > (w/h)_{cr}$. Consequently, Strouhal numbers determined from present study for $0.5 \leq w/h \leq 2.0$ decrease with increasing w/h. Data determined from present study at zero incidence and data from the literature (see Refs. 13, 14, and 33–36) are compared in Table 1.

The effects of the incidence angles on the Strouhal number Sr for rectangular cylinders are presented in Fig. 22 along with some data from the literature.[12,35,37] As is seen, the Strouhal number first increases and reaches the maximum values then decreases with increasing the angle of incidence. Strouhal numbers reach to maximum values at a certain value of the angle of incidence. Measurements by several authors of vortex-shedding frequency for square section cylinder[12] show that, as the incidence is increased from 0 deg, the Strouhal number first increases steadily then rises rather abruptly to a maximum just before $\alpha = 13.5$ deg.

Experimental work conducted on a square cylinder by Chen and Liu[35] shows that, at relatively small Reynolds numbers, 2×10^3–3×10^3, the Strouhal number increases to a maximum at 17-deg angle of incidence and then decreases gradually as Reynolds number increases from 3×10^3 to 8×10^3. At the higher Reynolds number, $Re = 8 \times 10^3$, α_{max}, at which the Strouhal number has its maximum value, remains steady at about 13 deg. In the present study, presented in Fig. 22, the Strouhal numbers reach maximums at about 14 and 10 deg for square ($w/h = 1$) and rectangular ($w/h = 1.6$) cylinders, respectively, in the Reynolds number range considered. Beyond these angles, the Strouhal numbers decrease with increasing angles of incidences. Thus, the Strouhal numbers are directly correlated to the angle of incidence. The jump in Strouhal number has been associated with the reattachment of the separated shear layer.[12,38,39]

As mentioned earlier, sometimes vortex sheddings are defined by the shedding frequency parameter $F = f_s h^2/\nu$, as well as by the Strouhal number. The Strouhal numbers and shedding-frequency parameters determined for the circular and rectangular cylinders of $w/h = 0.5, 1.0$, and 2.0 vs the Reynolds numbers are logarithmically presented in Figs. 23–26.

Figure 23 shows the Strouhal number and shedding frequency parameter dependences on Reynolds number for the circular cylinder at $x/D = 2.2$ and two y/D locations in the wake. As shown in Fig. 23, Strouhal numbers obtained for the circular cylinder slightly decrease with increasing Reynolds number. The value of the Strouhal number

Table 1 Strouhal number for rectangular cylinders

Reference	w/h	Sr
Spalart and Leonard[34]	1	0.11
Nagano et al.[33]	0.5	0.161
	0.62	0.153
	1.0	0.142
Chen and Liu[35]	1	0.137
Stansby[14]	0.2	0.19
	0.6	0.17
	1.0	0.13
Inamuro and Adachi[13]	1	0.14
Present study	0.5	0.16
	1.0	0.14
	1.6	0.1
	2.0	0.085
Chein and Chung[36]	Flat plate	0.14

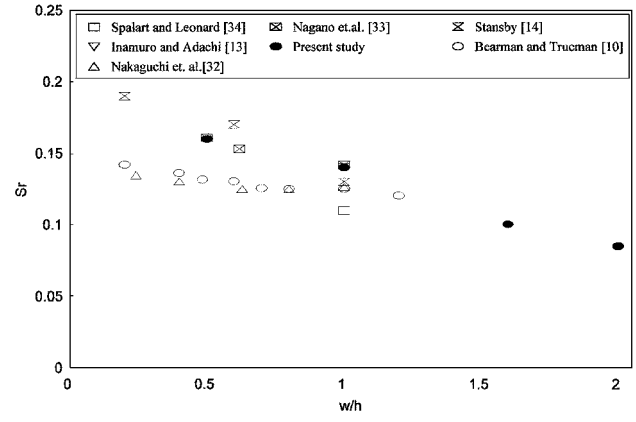

Fig. 21 Influence of *w/h* ratio on Strouhal number.

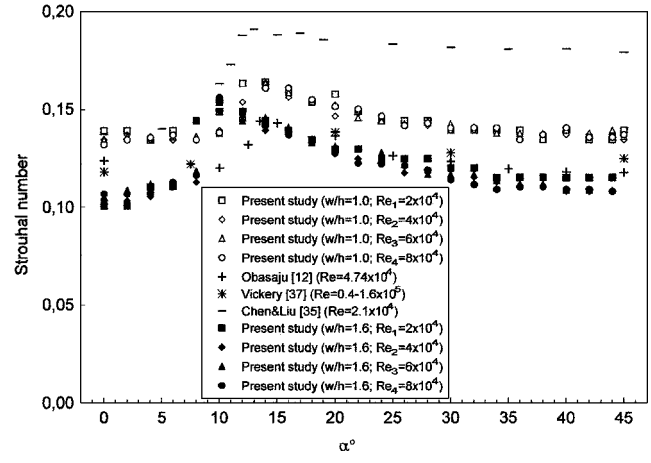

Fig. 22 Influence of angle of incidence on Strouhal number for the square cylinder.

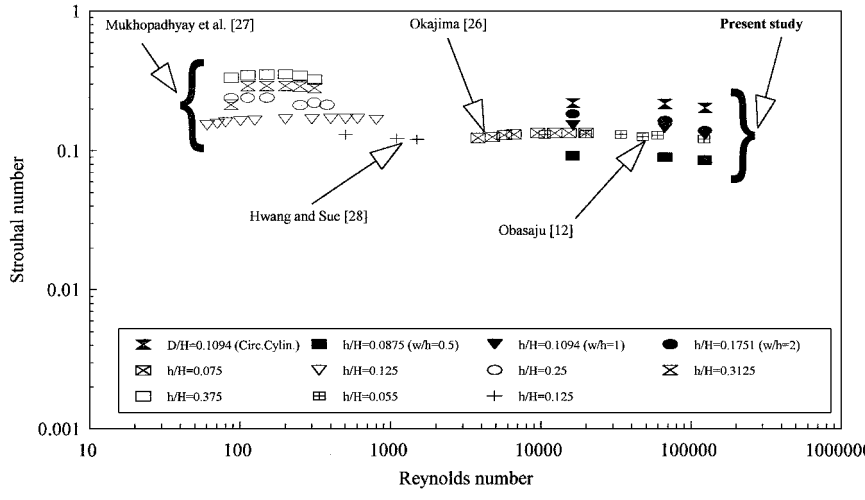

Fig. 20 Comparison of Strouhal numbers obtained at 0-deg incidence for square and rectangular cylinders with results from the literature.

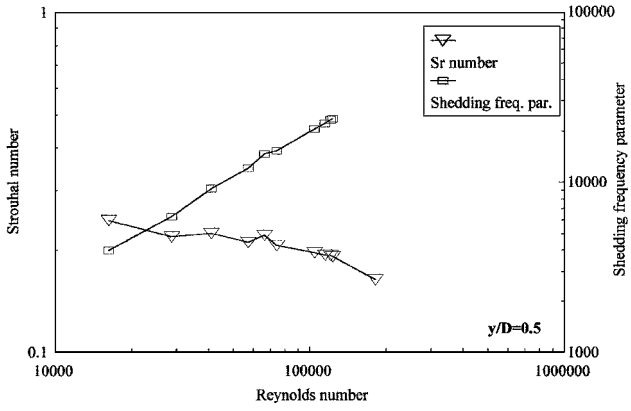

a) $y/D = 0.5$

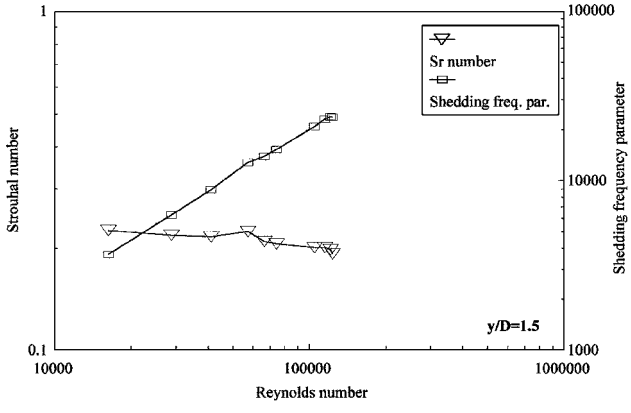

b) $y/D = 1.5$

Fig. 23 Strouhal numbers and shedding frequency parameters vs Reynolds number at $x/D = 2.2$ in the wake of the circular cylinder.

is about 0.2 until approximately $Re = 1.5 \times 10^5$, and then it considerably decreases after this value of Reynolds number (Fig. 23a). This is because critical flow begins after approximately $Re = 1.5 \times 10^5$.

The vortex-shedding frequency parameter varies almost linearly with Reynolds number in logarithmic scales. This increase agrees with the results in the literature. An empirical formula relating the nondimensional frequency (shedding frequency parameter) with Reynolds number for $1.6 \times 10^4 < Re < 1.24 \times 10^5$ was obtained as

$$F = f_s D^2/\nu = 0.181Re + 1539 \tag{3}$$

Figures 24–26 show the Strouhal number and shedding frequency parameter vs Reynolds number obtained for rectangular cylinders. The effects of the angle of incidence on the vortex shedding for these three models are also seen in Figs. 24–26. The shedding frequency parameter varies almost linearly with the Reynolds number in the logarithmic scale.

The correlation formulas of the shedding frequency parameters for rectangular cylinders with the Reynolds number were deduced from the experimental data for $w/h = 0.5$ as

$$F = f_s h^2/\nu = 0.135Re + 1819$$

$$2.6318 \times 10^4 < Re < 1.99427 \times 10^5 \tag{4}$$

for $w/h = 1.0$ as

$$F = f_s h^2/\nu = 0.116Re + 1191$$

$$1.6 \times 10^4 < Re < 1.24 \times 10^5 \tag{5}$$

and for $w/h = 2.0$ as

$$F = f_s h^2/\nu = 0.084Re + 124$$

$$1.3159 \times 10^4 < Re < 9.9714 \times 10^4 \tag{6}$$

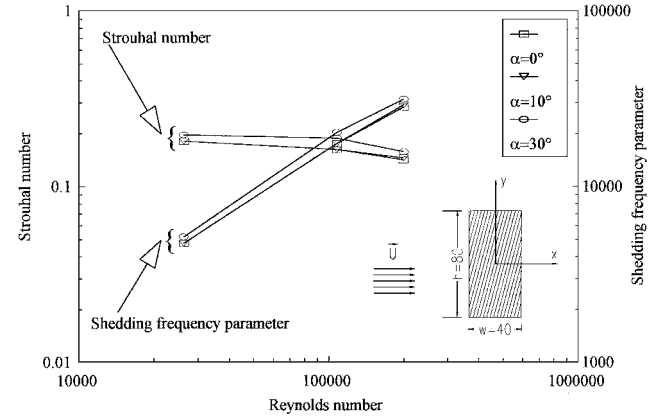

Fig. 24 Strouhal number and shedding frequency parameter vs Reynolds number at $x/h = 2.5$ in the wake of the rectangular cylinder $w/h = 0.5$ at 0-, 10-, and 30-deg incidence at $y/h = 0.3125$.

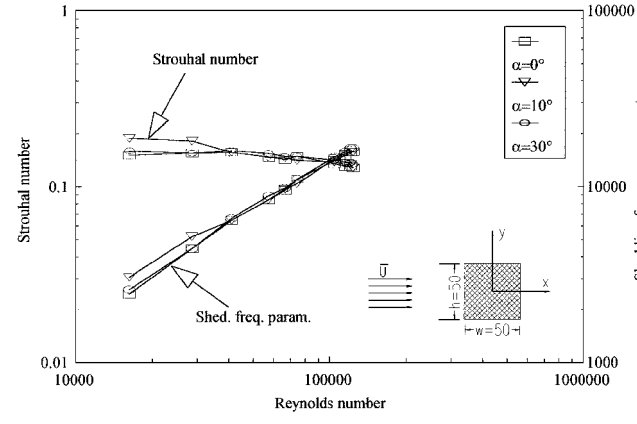

Fig. 25 Strouhal number and shedding frequency parameter vs Reynolds number at $x/h = 4$ in the wake of the square cylinder $w/h = 1$ at 0-, 10-, and 30-deg incidence at $y/h = 1.5$.

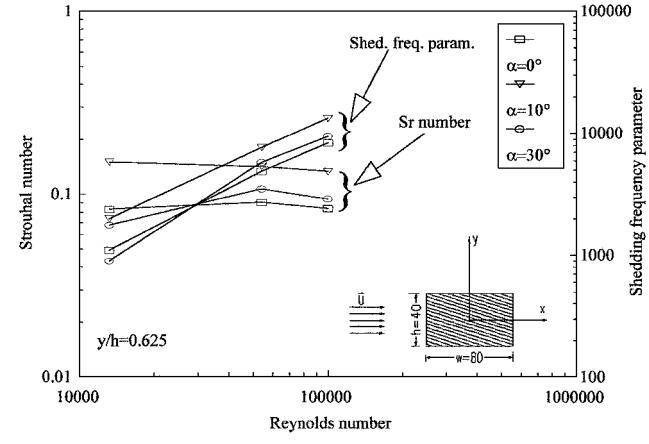

Fig. 26 Strouhal number and shedding frequency parameter vs Reynolds number at $x/h = 5$ in the wake of the rectangular cylinder $w/h = 2$ at 0-, 10-, and 30-deg incidence at $y/h = 0.62$.

IV. Conclusions

The flows around circular and rectangular cylinders were experimentally investigated over the Reynolds number range $1.3 \times 10^4 < Re < 2.0 \times 10^5$. The distributions of turbulence intensity measured in the wake of the circular cylinder have two peaks near the center of the wake at small x/D values ($x/D = 2.2$), whereas they have parabolic profiles at larger x/D values. The turbulence intensity profiles have maximums at the values approximately $y/D = \pm 0.5$ at $x/D = 2.2$, whereas they have a maximum at the value $y/D = 0$ at $x/D = 5.8$ and 14.8. The distributions of turbulence intensity measured in the wake of the square cylinder have two peaks at

three stations, $x/h = 2.2$, 5.8, and 14.8 for $Re = 1.467 \times 10^4$. As Reynolds number increases, these two peaks diminish, and turbulence intensity profiles have maximum values on the centerline of the wake. When turbulence intensity profiles for the circular and square cylinder models with the same hydraulic diameter are compared, the turbulence intensity of the flow and width of the wake around the square model are higher than those around the circular model due to their different geometries and different separation points.

Over the range $1.6024 \times 10^4 \leq Re \leq 1.33687 \times 10^5$, the surface pressure coefficient C_p measured on the circular cylinder has a maximum value at the front stagnation point and then decreases with the circumferential angle, reaching the minimum value at about $\theta = 70$ deg. Hence, pressure coefficient varies in the front of the cylinder and becomes considerably uniform in the rear side of the cylinder ($90 \leq \theta \leq 270$ deg).

The highest pressures measured on the square cylinder were obtained on the front face that is normal to the flow in the incidence 0 deg. As the incidence was increased from 0 to 30 deg, because the flows on the front and bottom surfaces were compressed, the pressures on these surfaces changed strongly. The pressures on surfaces that remain in the separated flow region almost did not change.

In the spectral measurements made in the wake of the circular cylinder model, vortex shedding was detected over the range $0.3 \leq y/D < 1.5$ at $x/D = 2.2$, whereas it was not detected in the region of $y/D \geq 1.5$. Dominant peaks were detected at $y/D = 0.3$ and 1.0 for $Re = 1.6279 \times 10^4$ and one dominant peak was detected at $y/D = 0.5$ for $Re = 6.6539 \times 10^4$ and 1.23355×10^5 at $x/D = 2.2$ in the wake of the circular cylinder. Depending on the location at which the spectral measurement take place, the magnitude of the spectral peaks varies with the Reynolds number.

In the spectral measurements calculated in the wake of the square cylinder model, dominant spectral peaks were detected at $y/h = 1$ for the Reynolds numbers 1.6279×10^4, 6.6539×10^4, and 1.23355×10^5 at 0- and 10-deg incidences but at $y/h = 0.5$ for the same Reynolds numbers at 30-deg incidence.

Strouhal numbers measured for the circular cylinder were a little above the value 0.2 for the Reynolds number range $Re < 8 \times 10^4$, whereas they were approximately the value 0.2 for the Reynolds number range $8 \times 10^4 < Re < 1.5 \times 10^5$. The Strouhal number slightly decreases as the Reynolds number increases. Nondimensional frequency (shedding frequency parameter) determined from spectral density functions increased linearly with Reynolds number in logarithmic scale.

Strouhal number decreases with increasing w/h ratio for rectangular cylinders in the range of $0.5 < w/h < 2.0$. When Strouhal numbers obtained for both circular and square cylinders with the same hydraulic diameter and blockage ratio are compared, the Strouhal numbers for the circular cylinder are approximately 50% higher than those of square cylinder. The shedding frequency parameter varies almost linearly with the Reynolds number in the logarithmic scale.

The Strouhal number of the rectangular cylinder increases with increasing angle of incidence and reaches to its maximum value at about $\alpha = 14$ deg for the square cylinder and $\alpha = 10$ deg for the rectangular cylinder, $w/h = 1.6$, and then decreases with increasing angle of incidence. The increase in Strouhal number with the angle of incidence might be due to the reattachment point of the boundary layer.

References

[1]Tritton, D. J., "Experiments on the Flow Past a Circular Cylinder at Low Reynolds Numbers," *Journal of Fluid Mechanics*, Vol. 6, 1959, pp. 547–567.

[2]Gerrard, J. H., "The Mechanics of the Formation Region of Vortices Behind Bluff Bodies," *Journal of Fluid Mechanics*, Vol. 25, 1966, pp. 401–413.

[3]Gaster, M., "Vortex Shedding from Circular Cylinders at Low Reynolds Numbers," *Journal of Fluid Mechanics*, Vol. 46, No. 4, 1971, pp. 749–756.

[4]Hunt, J. C. R., "A Theory of Turbulent Flow round Two-Dimensional Bluff Bodies," *Journal of Fluid Mechanics*, Vol. 61, No. 4, 1973, pp. 625–706.

[5]Sakamoto, H., and Arie, M., "Vortex Shedding from a Rectangular Prism and a Circular Cylinder Placed Vertically in a Turbulent Boundary Layer," *Journal of Fluid Mechanics*, Vol. 126, 1983, pp. 147–165.

[6]Meroney, R. N., "Wind-Tunnel Modeling of the Flow About Bluff Bodies," *Journal of Wind Engineering and Industrial Aerodynamics*, Vol. 29, 1988, pp. 203–223.

[7]Yokoi, Y., Saito, S., Kamemoto, K., and Ogawa, Y., "Vortex Shedding From a Circular Cylinder in a Pipe," *Nippon Kikai Gakkai Ronbunshu, B Hen*, Vol. 57, No. 544, 1991, pp. 4011–4015.

[8]Murakami, S., Mochida, A., Hayashi, Y., and Sakamoto, S., "Numerical Study on Velocity-Pressure Field and Wind Forces for Bluff Bodies by k–ε, ASM and LES," *Journal of Wind Engineering and Industrial Aerodynamics*, Vol. 41–44, 1992, pp. 2841–2852.

[9]Huang, X. Y., "Feedback Control of Vortex Shedding from a Circular Cylinder," *Experiments in Fluids,* Vol. 20, No. 3, 1996, pp. 218–224.

[10]Bearman, P. W., and Trueman, D. M., "An Investigation of the Flow Around Rectangular Cylinders," *Aeronautical Quarterly*, Vol. 23, Aug. 1972, pp. 229–237.

[11]Petty, D. G., "The Effect of Turbulence Intensity and Scale on the Flow Past Square Prisms," *Journal of Industrial Aerodynamics*, Vol. 4, 1979, pp. 247–252.

[12]Obasaju, E. D., "An Investigation of the Effects of Incidence on the Flow Around a Square Section Cylinder," *Aeronautical Quarterly,* Vol. 34, Nov. 1983, pp. 243–259.

[13]Inamuro, T., and Adachi, T., "Numerical Flow Simulation for Wind Engineering," *Journal of Wind Engineering*, Vol. 28, 1984, pp. 29–44.

[14]Stansby, P. K., "A Generalized Discrete-Vortex Method for Sharp-Edged Cylinders," *AIAA Journal*, Vol. 23, No. 6, 1985, pp. 856–861.

[15]Nakamura, Y., Ohya, Y., and Ozono, S., "The Effects of Turbulence on Bluff-Body Mean Flow," *Journal of Wind Engineering and Industrial Aerodynamics,* Vol. 28, 1988, pp. 251–259.

[16]Park, W. C., "Computation of Flow Past Single and Multiple Bluff Bodies by a Vortex Tracing Method," Ph.D. Dissertation, Fluid Mechanics, Univ. of Minnesota, Minneapolis, MN, March 1989.

[17]Durao, D. F. G., Gouveia, P. S. T., and Pereira, J. C. F., "Velocity Characteristics of the Flow Around a Square Cross Section Cylinder Placed Near a Channel Wall," *Experiments in Fluids*, Vol. 11, 1991, pp. 298–304.

[18]Kelkar, K. M., and Patankar, S. V., "Numerical Prediction of Vortex Shedding Behind a Square Cylinder," *International Journal for Numerical Methods in Fluids*, Vol.14, 1992, pp. 327–341.

[19]Bosch, G., and Rodi, W., "Simulation of Vortex Shedding Past a Square Cylinder Near a Wall," *International Journal of Heat and Fluid Flow*, Vol. 17, No. 3, 1996, pp. 267–275.

[20]Roshko, A., "Experiments on the Flow Past a Circular Cylinder at Very High Reynolds Number," *Journal of Fluid Mechanics*, Vol. 78, 1961, pp. 561–576.

[21]Farell, C., and Blessmann, J., "On Critical Flow Around Smooth Circular Cylinders," *Journal of Fluid Mechanics*, Vol. 136, 1983, pp. 375–391.

[22]West, G. S., and Apelt, C. J., "The Effects of Tunnel Blockage and Aspect Ratio on the Mean Flow Past a Circular Cylinder with Reynolds Numbers Between 10^4 and 10^5," *Journal of Fluid Mechanics*, Vol. 114, 1982, pp. 361–377.

[23]Blackburn, H. M., and Melbourne, W. H., "The Effect of Free-Stream Turbulence on Sectional Lift Forces on a Circular Cylinder," *Journal of Fluid Mechanics*, Vol. 306, 1996, pp. 267–292.

[24]Mizota, T., and Okajima, A., "Experimental Studies of Mean Flow Around Rectangular Prisms," *Proceedings of the Japan Society of Civil Engineers*, Vol. 312, 1981, pp. 39–47 (in Japanese).

[25]Mizota, T., and Okajima, A., "Experimental Studies of Unsteady Flow Around Rectangular Prisms," *Proceedings of the Japan Society of Civil Engineers*, Vol. 312, 1981, pp. 49–57 (in Japanese).

[26]Okajima, A., "Strouhal Numbers of Rectangular Cylinders," *Journal of Fluid Mechanics*, Vol. 123, 1982, pp. 379–398.

[27]Mukhopadhyay, A., Biswas, G., and Sundararajan, T., "Numerical Investigation of Confined Wakes Behind a Square Cylinder in a Channel," *International Journal for Numerical Methods in Fluids*, Vol. 14, 1992, pp. 1473–1484.

[28]Hwang, R. R., and Sue, Y. C., "Numerical Simulation of Shear Effect on Vortex Shedding Behind a Square Cylinder," *International Journal for Numerical Methods in Fluids*, Vol. 25, 1997, pp. 1409–1420.

[29]Ilday, O., Acar, H., Elbay, M. K., and Atli, V., "Wakes of Three Axisymmetric Bodies at Zero Angle of Attack," *AIAA Journal*, Vol. 31, No. 6, 1993, pp. 1152–1154.

[30]Achenbach, E., and Heinecke, E., "On Vortex Shedding From Smooth and Rough Cylinders in the Range of Reynolds Numbers From 6×10^3 to 5×10^6," *Journal of Fluid Mechanics*, Vol. 109, 1981, pp. 239–251.

[31] Bearman, R. W., "On Vortex Shedding From a Circular Cylinder in the Critical Reynolds Number Regime," *Journal of Fluid Mechanics*, Vol. 37, 1969, pp. 577–585.

[32] Nakaguchi, H., Hashimoto, K., and Muto, S., "An Experimental Study on Aerodynamic Drag of Rectangular Cylinders," *Journal of the Japan Society for Aeronautical and Space Sciences*, Vol. 16, 1968, pp. 1–5.

[33] Nagano, S., Naito, M., and Takata, H., "A Numerical Analysis of Two Dimensional Flow Past a Rectangular Prism by a Discrete Vortex Model," *Computers and Fluids*, Vol. 10, No. 4, 1982, pp. 243–259.

[34] Spalart, P. R., and Leonard, A., "Computation of Separated Flows by a Vortex Algorithm," AIAA Paper 81-1246, 1981.

[35] Chen, J. M., and Liu, C. H., "Vortex Shedding and Surface Pressures on a Square Cylinder at Incidence to a Uniform Air Stream," *International Journal of Heat and Fluid Flow*, Vol. 20, April 1999, pp. 592–597.

[36] Chein, R., and Chung, J. N., "Discrete-Vortex Simulation of Flow over Inclined and Normal Plates," *Computers and Fluids*, Vol. 16, No. 4, 1988, pp. 405–427.

[37] Vickery, B. J., "Fluctuating Lift and Drag on a Long Cylinder of Square Cross Section in Smooth and in Turbulent Stream," *Journal of Fluid Mechanics*, Vol. 25, 1966, pp. 481–494.

[38] Rockwell, D. O., "Organized Fluctuations due to Flow past a Square Cross Section Cylinder," *Journal of Fluids Engineering*, Vol. 99, 1977, pp. 511–516.

[39] Knisely, C. W., "Strouhal Numbers of Rectangular Cylinders at Incidence: A Review and New Data," *Journal of Fluids and Structures*, Vol. 4, 1990, pp. 371–393.

P. R. Bandyopadhyay
Associate Editor